HAL
open science

Strong tectonic and weak climatic control on exhumation rates in the Venezuelan Andes

Mauricio M.A. Bermúdez, Pieter van Der Beek, Matthias Bernet

To cite this version:

Mauricio M.A. Bermúdez, Pieter van Der Beek, Matthias Bernet. Strong tectonic and weak climatic control on exhumation rates in the Venezuelan Andes. Lithosphere, 2013, 5 (1), pp.3-16. 10.1130/L212.1 . hal-00781638

HAL Id: hal-00781638

https://hal.science/hal-00781638v1

Submitted on 28 Jan 2013

HAL is a multi-disciplinary open access archive for the deposit and dissemination of scientific research documents, whether they are published or not. The documents may come from teaching and research institutions in France or abroad, or from public or private research centers.

L'archive ouverte pluridisciplinaire **HAL**, est destinée au dépôt et à la diffusion de documents scientifiques de niveau recherche, publiés ou non, émanant des établissements d'enseignement et de recherche français ou étrangers, des laboratoires publics ou privés.

Strong tectonic and weak climatic control on exhumation rates in the Venezuelan Andes

Mauricio A. Bermúdez[a,b], Peter A. van der Beek[b], Matthias Bernet[b]

[a]Laboratorios de Termocronología y Geomatemáticas, Escuela de Geología, Minas y Geofísica. Facultad de Ingeniería, Universidad Central de Venezuela, Caracas, Venezuela. (mauricio.bermudez@ing.ucv.ve/ Fax: +58 212 6053120/ Phone: +58 212 6053123)

[b]Institut des Sciences de la Terre (ISTerre), Université Joseph Fourier, CNRS, BP 53, 38041 Grenoble cedex 9, France.

6310 Words

7 Figures, 3 Tables

83 References

ABSTRACT

We have studied the relationships between present day relief, precipitation, stream power, seismic energy, seismic strain rate and long-term exhumation rates for the Venezuelan Andes. Average long-term exhumation rates were determined for seven large catchments in the Venezuelan Andes from fission-track analysis of detrital apatite. A quantitative comparison between eight new detrital apatite fission-track (AFT) age distributions presented here and previously published bedrock AFT age patterns shows that detrital AFT ages can be used for predicting exhumation patterns across the mountain belt. Catchment-averaged exhumation rates estimated from the raw data range from 0.48±0.02 to 0.80±0.26 km Myr^{-1}. Accounting for variable sediment yield and assuming that short-term sediment production rates scale with long-term exhumation rates, these rates vary from 0.33±0.07 to 0.48±0.08 km Myr^{-1}. No variation in rates is observed between the northwestern and southeastern flanks of the mountain belt, despite a threefold increase in precipitation from the northwest to the southeast. Long-term exhumation rates are strongly correlated with relief in the different catchments, but no or negative correlations exist with precipitation data or present-day erosion indexes, while the correlation with seismic energy released by earthquakes is weak to moderate. This lack of correlation may be caused by the insufficient temporal range of the available precipitation and seismicity data, and the different time scales involved in the comparison. Long-term exhumation rates are, however, strongly correlated with seismic strain rates (which take the temporal earthquake magnitude-frequency scaling into account), suggesting that the moderate correlation with seismic energy is indeed related to the different timescales and that tectonic control on exhumation is significant. In contrast, given that precipitation patterns in the Venezuelan Andes should have been installed during Miocene

times, we suggest that decoupling of relief and exhumation from present-day climate explains the lack of correlation between exhumation and precipitation.

Keywords: Venezuelan Andes, detrital apatite fission-track, exhumation, erosion rates, relief, climate.

1. INTRODUCTION

The relative importance of tectonic and climatic control on relief development and exhumation in mountain belts remains strongly debated (e.g., Molnar and England, 1990; Burbank et al., 2003; Reiners et al., 2003; Strecker et al., 2009; Champagnac et al., 2012). Problems limiting our ability to discriminate between the driving forces for the development of topography and erosion include the limited temporal precision with which variations in exhumation rate, climate and tectonics can be resolved and compared (e.g., Whipple, 2009), and the different temporal scales for which we have records of these processes (Burbank et al., 2003; Reiners et al., 2003; Vernon et al., 2009). While thermochronologic data record denudation on million-year timescales, seismicity (arguably a proxy for the intensity of at least brittle tectonics) and precipitation records (an admittedly reductionist climate descriptor) generally do not go back more than a few decades. Nevertheless, the comparison of spatial patterns of long-term exhumation rates and short-term seismicity and precipitation may provide some first-order insights into the processes driving exhumation, even in the absence of strong spatial correlations (Finlayson et al., 2002; Dadson et al., 2003; Koons, 2009; Vernon et al., 2009).

The Andes are important in the discussion on climate versus tectonic controls on topography and exhumation in mountain belts because of the obvious link between laterally varying

topographic characteristics and climatic zonation (e.g., Montgomery et al., 2001; Lamb and Davies, 2003), as well as the strong asymmetry in orographic precipitation associated with this orogen (e.g., Bookhagen and Strecker, 2008). While many studies have concentrated on the southern and central Andes (e.g., Strecker et al., 2007; Farías et al., 2008; Thomson et al., 2010), attention has recently also focused on the northern Andes. Mora et al. (2008), for instance, describe strongly asymmetric deformation and exhumation patterns in the eastern Colombian Andes, which they link to the strong NW-SE precipitation gradient across this part of the mountain belt. In contrast, Mora et al. (2009) and Parra et al. (2009) argue for a strong control of inherited crustal structure on spatio-temporal patterns of exhumation and relief production.

In this study, we present new detrital apatite fission-track (AFT) data from eight river catchments in the Venezuelan Andes, the north-easternmost extension of the Northern Andes. We compare the detrital AFT data to available bedrock AFT data of the Venezuelan Andes (Kohn et al., 1984; Bermúdez et al., 2010, 2011) in order to test whether they faithfully record exhumation in the catchments (e.g., Ruhl and Hodges, 2005; Brewer et al., 2006) and to spatially integrate the still relatively sparse *in-situ* data. The objective of this study is to examine the relative control of climate and tectonics on exhumation and relief development in the Venezuelan Andes. For this purpose, long-term exhumation rates derived from the detrital thermochronology data are compared to present-day relief, precipitation rates, seismic energy release, seismic strain rate and short-term erosion potential predicted from the average stream power of individual drainages.

2. GEOLOGIC SETTING

The Venezuelan Andes were formed by oblique convergence between the continental Maracaibo block and the South American plate, driven by eastward movement of the Caribbean plate (Fig. 1A; Case et al., 1990). The orogen is characterized by high seismicity and spatially variable exhumation since Miocene times, as recorded by AFT thermochronology data (Kohn et al., 1984; Bermúdez et al., 2010, 2011). The structure of the Venezuelan Andes is controlled by reactivated faults that delineate individual tectonic blocks (Fig. 1B). These faults were inherited from Early Mesozoic rifting, and possibly from earlier orogenesis (Aleman and Ramos, 2000; Pindell and Kennan, 2001). Bermúdez et al. (2010) defined at least seven tectonic blocks with contrasting exhumation and cooling histories, separated by major strike-slip and thrust faults. The orogen is bounded by two seismically active thrust belts to the northwest and southeast (Coletta et al., 1997). The most important strike-slip fault systems are the right-lateral Boconó, Central-Sur Andino and Caparo faults and the left-lateral Icotea, Valera, and Burbusay or Carache fault systems (Fig. 1B). The Boconó fault zone extends from the border with Colombia for more than 500 kilometers to the northeast (Fig. 1) and divides the Venezuelan Andes symmetrically in its central part into two separate chains; the Sierra La Culata to the northwest and the Sierra Nevada to the southeast. These two blocks cooled rapidly but diachronously during the late Miocene–Pliocene (Kohn et al., 1984; Bermúdez et al., 2011). In contrast, the Caparo and Trujillo blocks (Fig. 1B), at the southwestern and northeastern ends of the Venezuelan Andes respectively, experienced slow cooling from the late Oligocene - late Miocene onward (Bermúdez et al., 2010). Both these blocks are dominated by Paleozoic and Mesozoic sedimentary rocks, whereas Proterozoic to Paleozoic gneisses and granites are exposed in the core of the mountain belt, in the Sierra Nevada and Sierra La Culata ranges. This crystalline basement is covered by

Cenozoic sedimentary rocks of the Maracaibo and Barinas foreland basins to the north and south, respectively (Fig. 1).

3. DETRITAL APATITE FISSION-TRACK THERMOCHRONOLOGY

Thermochronology of detrital minerals allows quantifying cooling rates and exhumation processes in convergent mountain belts (e.g., Garver et al., 1999; Carter, 2007), providing a complimentary record of the erosional history of a mountain belt with respect to local cooling paths deduced from *in-situ* samples within the orogen (Brandon and Vance, 1992). Detrital thermochronology applied to modern river sediments provides a spatially integrated view of the exhumation history of an entire drainage basin, which may be the only way to characterise exhumation patterns for inaccessible areas.

3.1. Data collection and discrimination of age components

We collected samples for detrital AFT thermochronology from eight river catchments draining the Venezuelan Andes. The Coloncito, Tucaní, San Pedro, Agua Viva, and Mimbós rivers drain the northern flank, the Chama and Chejendé rivers drain the central range, and the Santo Domingo River drains the southern flank of this mountain belt (Fig. 2). Samples were collected along active river channel bars at all sites and prepared using standard techniques (cf. Bermúdez et al., 2010). We aimed at dating at least 100 grains per sample in order to attain statistically significant AFT age populations. This objective was attained for 5 out of 8 samples (Table 1).

Because apatites in detrital samples are derived from different sources with variable bedrock ages within a drainage area, the grain-age distribution may contain several grain-age

components (Brandon and Vance, 1992; Garver et al., 1999). Different methods have been proposed for decomposing a fission-track grain age distribution into its age components, the most popular of which has become the binomial peak-fitting method (e.g. Galbraith and Green, 1990; Brandon 1992, 1996). Here, we use this method (as described by Stewart and Brandon, 2004) to decompose the grain-age distributions of our modern river samples. Resulting age peaks are reported in Table 1 and Figure 2. All samples except 1707 from the Tucaní catchment record a Late Miocene (6-10 Ma) age peak, and all except those from the northwestern-most catchments (Agua Viva and Chejendé) also record a Mio-Pliocene (2.5-6 Ma) age peak. Although all samples contain older (15-35 Ma) single-grain ages, only the Santo Domingo, Agua Viva, Tucaní and Chama catchments record an older (Early-Middle Miocene; 14-25 Ma) age peak. The Late Miocene age population is dominant (57 to 100%) in most samples, except for the Santo Domingo and Coloncito catchments where the younger (Mio-Pliocene) age population is larger. In the Tucaní sample, 90% of the grains are grouped in a 5.9±0.7 Ma age peak. The Chejendé River is a tributary of the Agua Viva and drains part of its catchment (Fig. 1); for this reason we merged the detrital data for the corresponding samples (0507 and 0807) and proceed to apply the decomposition of the grain-age distribution as above. The resulting age peaks are very similar to those from the Agua Viva sample alone (Table 1).

Access to the southern flank of the Venezuelan Andes is difficult and our dataset contains only one river draining to the south. The Santo Domingo River sample shows a similar grain-age distribution and peak ages as the rivers that drain to the north (Table 1, Figure 2), although the component ages are slightly older than corresponding age peaks in the other samples.

Although binomial peak fitting provides a convenient means of analyzing detrital thermochronology data, it may mask similarities in age structure between different samples. In order to analyze these, we use the Kolmogorov-Smirnov and Kuiper tests (Conover, 1980) to quantitatively compare the detrital age probability density functions (PDF) for the seven catchments (cf. Supplementary Material; Figure S1 and Table S1). These comparisons indicate that, at a 95% confidence level, the samples from four catchments located in the central part of the Venezuelan Andes (Chama, Tucaní, Santo Domingo and San Pedro) yield a similar detrital age distribution, while the age distributions of the other samples are significantly different from each other.

3.2. Comparison of detrital and bedrock AFT ages

Previous studies have shown that detrital thermochronology faithfully records source-area exhumation in a number of different settings (e.g. Bernet et al., 2004; Ruhl and Hodges, 2005; Brewer et al., 2006). Here, we compare our detrital AFT grain-age distributions of an individual drainage to previously published bedrock AFT ages. We analyse the Chama catchment, as it is the only one within the Venezuelan Andes for which sufficient *in-situ* data (Kohn et al. 1984; Bermúdez et al., 2011) are currently available to derive a reliable bedrock age map.

Several authors (Stock et al., 2006; Vermeesch, 2007; McPhillips and Brandon, 2010) have developed quantitative methods for comparing bedrock and detrital age patterns. We adopt the approach described by Vermeesch (2007), randomly sampling a number of ages equal to the number of single-grain ages in the detrital sample from the interpolated bedrock age map (see Glotzbach et al., in review for details). This method has the advantage that it takes into account Poisson-distributed measurement uncertainties. We sample the bedrock age

distribution and construct the predicted age probability-density function (PDF) and cumulative-density function (CDF) 1000 times (Fig. 3a). We then use the Kolmogorov-Smirnov (KS) (Conover, 1980) and Kuiper equality tests (Ruhl and Hodges, 2005) to compare the predicted AFT CDFs and PDFs with the detrital AFT data. Additional simulations (5000; 10000) do not change the statistical results of our comparison. The resulting average *p*-values show that the inferred bedrock age distribution is significantly different from the detrital age distribution at the 95% confidence level; all simulations fail the Kuiper test and the vast majority also fail the KS test.

There are several possible reasons for this discrepancy. First, we do not take into account potential variations in apatite content for different lithologies in the catchment, whereas this may strongly influence the detrital age distribution (e.g., Tranel et al., 2011). However, (1) we have no information on the relative apatite abundance in different rock types of the Venezuelan Andes, (2) the sampled Chama catchment is mainly underlain by relatively homogeneous Precambrian basement rocks (see Chama River in Fig. 1B).

Another possibility is that the catchment is not currently eroding at a uniform rate, which is an inherent assumption when randomly picking ages from the interpolated bedrock age distribution. It is relatively simple to weight the bedrock age distribution according to a model of inferred present-day erosion rates (Vermeesch, 2007; McPhillips and Brandon, 2010; Glotzbach et al., in review). Here we assume that the short-term erosion rates in the catchment are coupled to the long-term exhumation rates, which can be estimated from the AFT ages using a simple 1D thermal model (cf. next section). We thus resample the interpolated bedrock age distribution, letting the probability of sampling any particular age be determined by the long-term exhumation rate associated with that age, relative to the average long-term

exhumation rate of the catchment. The resulting predicted CDF's/PDF's compare very favourably to the observed detrital AFT age distribution (Fig. 3B); both the KS and Kuiper tests suggest the two distributions are similar at the 95% confidence level.

We conclude from the above comparisons that the detrital AFT age distributions provide a reliable estimate of *in-situ* bedrock ages in the sampled catchments when weighted by their associated long-term exhumation rates, implying that the apatite yield of the catchment (as recorded by our detrital samples) is controlled by the long-term exhumation rates.

3.3. Long-term exhumation rates

The detrital age distributions can be used to provide predictions of average long-term exhumation rates of individual drainages, which can be compared to potential tectonic or climatic control parameters. We employ a simple 1-D steady-state thermal model developed by Brandon et al. (1998; see also Ehlers, 2005; Reiners and Brandon, 2006) to convert detrital AFT ages to exhumation rates. As this model does not take either transient thermal effects (e.g. Rahl et al., 2007) or the 3-D effects of topography (e.g., Whipp et al., 2009) into account, predicted exhumation rates should be considered as first-order estimates. Parameters used for these calculations are a surface temperature of 25°C, layer thickness to constant temperature of 40 km, thermal diffusivity of 25 km^2 My^{-1}, heat production of 10 °C My^{-1} and a temperature at the base of the layer of 700 °C (see Bermúdez et al., 2011 for details). The last two values were constrained by inverse modeling of age-elevation relationships in the central Venezuelan Andes (Bermúdez et al., 2011) and imply a pre-exhumation surface geothermal gradient close to 25 °C km^{-1}. The model iteratively calculates an exhumation rate (ε), cooling rate, closure-temperature (T_c) and -depth (z_c) from the AFT ages, using the Dodson (1973)

equation to solve for the closure temperature of the AFT thermochronometer and a steady-state thermal structure to relate this to the closure depth.

For each detrital sample, we use the above procedure to translate single-grain ages into exhumation rates, which we then combine to predict a catchment-wide average long-term exhumation (ε_T) rate as:

$$\varepsilon_T = \frac{1}{N}\sum_{j=1}^{N}\varepsilon_j \tag{1}$$

where ε_j is the exhumation rate inferred for grain j and N is the total number of grains in the detrital sample. In order to include the expected effect that rapidly exhuming areas of a catchment will contribute more sediment (and thus more datable apatite grains), as indicated by the comparison of bedrock and detrital age distributions in the previous section, we also calculate a weighted long-term catchment-averaged exhumation rate $(\varepsilon_T)_w$:

$$(\varepsilon_T)_w = \frac{N}{\sum_{j=1}^{N}\frac{1}{\varepsilon_j}} \tag{2}$$

Results are reported in Table 2. Catchment-averaged exhumation rates vary between 0.48±0.02 km Myr^{-1} for the Santo Domingo and 0.80±0.26 km Myr^{-1} for the Mimbós catchments. As expected, weighted-average rates are lower, and all weighted long-term exhumation rates in the Central Venezuelan Andes overlap within error, varying between 0.33±0.07 (Agua Viva-Chejendé) and 0.48±0.08 (Coloncito) km Myr^{-1}. The northeastern Agua Viva/Chejendé catchment shows the lowest long-term exhumation rates (< 0.35 km Myr^{-1}). The central Chama and Santo Domingo catchments show intermediate rates (0.35-0.40 km Myr^{-1}) and the catchments located on the northwestern flank of the range show the highest exhumation rates (> 0.40 km Myr^{-1}). In the following discussion, we will focus on the

weighted-average catchment exhumation rates, which we consider to be the most reliable estimates.

4. POTENTIAL CONTROLLING PARAMETERS

In order to explore the potential topographic, tectonic or climatic controls on the exhumation rates determined above, we derive quantitative measures for these controls (relief, precipitation, seismicity, stream power) in the following sections.

4.1. Elevation and Relief

The Venezuelan Andes rise from sea level at Lake Maracaibo, to the north of the mountain belt, to close to 5000 m elevation at Pico Bolívar in the Sierra Nevada Block (Fig. 1B). This part of the Andes most probably emerged as an orographic barrier at about 8 Ma (Hoorn et al., 1995; Bermúdez et al., 2011). The central Sierra Nevada and Sierra la Culata ranges (Fig. 1C) include more than 60 peaks with elevations of 4300 m and above (Fig 4A). These highest parts of the Venezuelan Andes were glaciated during the Quaternary. Moraines of the Last Glacial Maximum are encountered at 3400-3600 m elevation (Schubert, 1984), with older moraines occurring at elevations several hundred meters lower. The mean elevation of the range is significantly lower to the northeast and southwest, varying between 1160 and 1695 m (Bermúdez et al., 2010).

Relief was calculated as the maximum elevation difference within a variable radius, between 1 and 15 km, for every pixel in the digital elevation model (e.g., Montgomery and Brandon, 2002). There is a power-law relationship between average relief of the different catchments and the radius at which it was calculated, with scaling exponents around 0.5-0.6, characteristic

for low-latitude mountain belts (Champagnac et al., 2012). The present-day relief of the Venezuelan Andes for a 5-km radius is shown in Figure 4A. Highest relief values of close to 3500 m are found along the central Chama River valley, which follows the Boconó fault. Other areas of high relief are located on the northwestern and southeastern flanks of the mountain belt. Relief is much lower within the central Sierra Nevada and Sierra la Culata ranges and in the Caparo and Trujillo blocks in the southwest and northeast of the Venezuelan Andes (Fig. 1B, 4A). The former are characterized by extensive low-relief summit surfaces that show widespread evidence for glacial bevelling through cirque retreat (e.g., Mitchell and Montgomery, 2006; Foster et al., 2008), whereas the latter show subdued relief at lower mean elevations with widespread soil mantling of slopes.

4.2 Precipitation

The topography of the Venezuelan Andes generates a well-developed orographic precipitation pattern. Moist air masses from equatorial South America in the south need to rise in order to cross the Venezuelan Andes to the north, causing heavy precipitation on its southern flank, whereas the centre and northern flank of the belt are more arid. It has been proposed that the present-day precipitation and drainage system of the Venezuelan Andes started developing at about 8 Ma, in response to tectonically driven surface uplift (Hoorn et al., 1995; Bermúdez et al., 2011). We have used precipitation data from 30 meteorological stations in and around the Venezuelan Andes to elaborate a mean annual precipitation map for the past twenty years. Although these measurements do not record snowfall as accurately as rainfall, the vast majority of precipitation is rainfall in the low-latitude Venezuelan Andes. The database was compiled from different sources: (1) NOAA World Temperature – Precipitation dataset (http://bonnet19.cs.qc.edu:7778/pls/rschdata/rd_start.main); (2) published data (Stansell et al., 2006; Naranjo & Duque, 2004); (3) Bio-climatic net stations of Mérida

(http://www.cecalc.ula.ve/redbc/colecciones/colecciones_datos.html); and (4) data provided by Gerard Kopp (pers. comm.) of the Institute for Meteorology and Climate Research, University of Karlsruhe (Germany) for the Mérida Atmospheric Research Station at Pico Espejo (MARS). The present-day precipitation map shown in Figure 4B was compiled from these data using nearest-neighbor interpolation (Arya et al., 1998) and highlights the strong precipitation gradient between the northern and southern flanks of the Venezuelan Andes, with precipitation ranging from 1.6 to 3.4 m yr^{-1} on the southern flank as opposed to 0.09-1.1 m yr^{-1} on the northern flank. A particular feature is the arid patch that expands into the orogen between El Vigía and Mérida: hot dry winds from the north exploit the Chama River valley to penetrate deep into the orogen, generating a unique arid climate in this area (Fig. 4B). A remotely sensed (TRMM) precipitation dataset synthesized by Bookhagen and Strecker (2008) shows overall similar patterns, both qualitatively and quantitatively.

4.3. Seismicity

Historical and instrumental seismicity in the Venezuelan Andes is strongly concentrated along the Boconó fault system. Smaller seismic events are scattered within a band of several tens of km width adjacent to this fault zone, indicating that many of the fault branches are also active (Fig. 5A). However, most of the seismicity occurs along the main trace of the fault at an average depth of about 15 km. Larger seismic events tend to occur at greater depth to the northwest (Lake Maracaibo basin) and southeast (Barinas basin) of the surface trace of the Boconó fault, reaching more than 40 km depth (Dewey, 1972, Niu et al., 2007). A seismic zone of intermediate depth (~160 km) occurs towards the southwestern boundary of the Venezuelan Andes and continues below the Eastern Cordillera of Colombia. This significant concentration of events is known as the Bucaramanga seismic nest (Schneider et al, 1987) and occurs within the subducted Caribbean slab below northern South America (van der Hilst and

Mann, 1994). More scattered, but relatively high magnitude ($M > 5$) earthquakes are associated with the north-south oriented Icotea, Valera and Burbusay fault systems to the north of the Venezuelan Andes (Fig. 5A).

Focal mechanisms suggest predominantly right-lateral faulting along the Boconó fault, left-lateral faulting along the north-south trending faults to the north of the Venezuelan Andes, and orthogonal thrusting along the northwest and southeast foreland fold-and-thrust belts (Colmenares and Zoback, 2003; Corredor, 2003; Cortés and Angelier, 2005). These focal mechanisms indicate a compressional stress regime with σ_1 oriented approximately WNW-ESE across the central Venezuelan Andes, evolving toward a strike-slip regime with a NW-SE directed σ_1 axis to the northeast. Studies of active tectonic landforms in the Venezuelan Andes, together with regional tectonic reconstructions, suggest that the current tectonic regime was installed during Pliocene-Quaternary times (Backé et al., 2006; Egbue and Kellogg, 2010).

In order to quantify the effects of seismicity across the Venezuelan Andes, we compiled a seismicity record over the last century (from January 1911 to January 2011), using data available from the digital library of the Geophysics Laboratory of Universidad de Los Andes, Mérida (http://lgula.ciens.ula.ve/) and data provided by the Venezuelan Foundation for Seismological Investigation (FUNVISIS; http://www.funvisis.gob.ve). The data were filtered using two criteria: (1) epicenters of earthquakes located between latitudes 72.25°W - 70.00°W and longitudes 7.75°N - 10.00°N; (2) only data with reported local magnitudes M_l were considered. Figure 5A shows a summary of earthquakes that occurred in the Venezuelan Andes during the last century. We calculated the released seismic energy (*Se*) from the local magnitudes using the classical expression of Gutenberg and Richter (1954):

$$\log(Se) = bM_l + a \approx 1.5M_l + 4.8 \quad (3)$$

The values of the parameters a and b are estimated by a least-squares fit of cumulative magnitude-frequency relationships constructed from subsamples of the seismic database for each catchment in 0.5º×0.5º cells and are equivalent to the intersect and slope, respectively, of the Gutenberg-Richter relationship (Gutenberg and Richter, 1954). Released seismic energy values were cumulated within circles with radius of 25 km around the epicenter of each earthquake. Figure 5B shows the resulting map of seismic energy obtained from this procedure. The rate of seismic energy release is highest in the central Venezuelan Andes (Chama catchment) and decreases toward the northeast and southwest. However, the calculated pattern is strongly affected by the $M_l > 5$ earthquakes that occurred on the Burbusay, Valera and Icotea fault systems.

The record of seismic energy release spans only 100 years, significantly shorter than the return period of major earthquakes in the Venezuelan Andes (300 years for $M \geq 7$ earthquakes; Audemard, 1997). Consequently, the pattern of released seismic energy may be locally underestimated. However, the seismicity records brittle deformation of the upper crust; the spatial distribution and frequency of earthquakes are intuitively related to the rate of brittle deformation (e.g. Holt et al., 2000). Thus, we can use the compiled seismic database to estimate the present-day distribution of brittle strain rate and extrapolate the total amount of seismic strain over timescales longer than the observation interval, using the observed earthquake magnitude-frequency (Gutenberg-Richter) relationship. To achieve this, we use the method described by Braun et al. (2009) and calculate seismic/brittle strain rate as:

$$\varepsilon_H = \left(\frac{1}{2\mu\Delta V\Delta t}\right)\left(\frac{b10^{a+9.1}}{1.5-b}\right)\left(10^{(1.5-b)M_{\max}}\right) \quad (4)$$

in which the parameters a and b are defined and calculated as explained above; M_{max} is the maximum observed magnitude; μ is elastic shear modulus; ΔV is the volume of the crust (that is, the moving 0.5º×0.5º cell area multiplied by depth of the maximum magnitude earthquake) in which the earthquakes were observed over a period of time Δt (in this case, Δt = 100 years). The depth of the maximum magnitude earthquakes (33-163 km) generally exceeds the depth of brittle-ductile transition (~15-20 km). Because we are using the seismic strain rate as a proxy for brittle deformation, we recalculated seismic strain rates using only earthquakes with hypocentral depths less than 20 km. However, we did not find any significant differences between the two approaches. The maximum-magnitude bin used in the least-squares fit always had at least one earthquake in it. Cells with a correlation coefficient, $r^2 < 0.95$ (mostly due to an incomplete catalogue) were not considered. In order to check the robustness of the results, we tested the effect of removing the minimum and maximum magnitude bins on the a and b values and the effect of forcing b to be exactly 1, but neither caused the seismic strain rate to change significantly.

Figure 5C shows the resulting map of seismic/brittle strain rate from subsamples (sliding 0.5 × 0.5° cells) of the seismic database for the Venezuelan Andes. The resulting seismic strain-rate map (Fig. 5C) shows maximum deformation occurring in the central and northwest Venezuelan Andes, with a second maximum occurring to the south of the mountain belt in the area of the 2001/12/21, M_w = 5.6 earthquake. Seismic strain rates vary between ~10^{-17} s^{-1} at the northeastern (Agua Viva-Chejendé catchment) and southwestern extremities of the belt, the latter influencing average seismic strain rates in the Chama catchment, and ~10^{-15} s^{-1} in the centre of the belt (Mimbós, San Pedro and Coloncito catchments).

4.4 Short-term erosion potential

The long-term exhumation rates estimated from detrital AFT ages can be compared to model predictions of the intensity of short-term erosion using the erosion-index approach of Finlayson et al. (2002). The erosion index (*EI*) can be calculated in different ways as a function of stream power, which is the rate of potential energy expenditure by flowing water and has been used extensively in studies of erosion, sediment transport, and geomorphology as a measure of the erosive power of rivers and streams (Wilson and Gallant, 2000; Wobus et al., 2006). The analysis is based on a prediction of bedrock incision rate as a function of stream power (Finlayson et al., 2002; Tucker and Whipple, 2002):

$$e = k \ A^m S^n \tag{5}$$

where e is the local incision rate, A is upstream drainage area (used as a proxy of discharge), S is local slope, and m, n and k are constants. The parameter k is mainly related to bedrock erodibility. Given the similar geologic and geographic conditions of the studied catchments and the lack of information on relative erodibility of the different lithologies outcropping in the Venezuelan Andes, we take k to be uniform throughout the study area. Setting k to unity, the predicted erosion index becomes:

$$EI = A^m \ S^n \tag{6}$$

Spatial variations in precipitation P can be incorporated into the prediction of EI in order to study their influence on spatial variability of the erosion potential:

$$EI_p = \sum \left[\left(A_p \right) P \right]^m S^n \tag{7}$$

where (A_p) is the pixel area, P is the local precipitation and the summation sign implies summing the along the flow-lines within the catchment in order to calculate the flow accumulation. We term EI_p the precipitation-modulated erosion index.

Different m and n values can be employed in equations (6) and (7), depending on the control of river incision rates by total stream power, stream power per unit channel width or shear stress (Finlayson et al., 2002; Tucker and Whipple, 2002). In the case where incision is controlled by total stream power (TSP), $m = n = 1$. For incision controlled by stream power per unit channel width (USP), $m = 1/2$ and $n = 1$. If incision is controlled by fluvial shear stress (SSP), $m = 1/3$ and $n = 2/3$.

Normalized erosion index maps for the Venezuelan Andes, predicted by the six possible models (TSP, USP, and SSP for uniform or spatially variable precipitation) are shown in Figure 6. These maps emphasize distinct zones of high erosion potential associated with the steepest terrain and largest discharge of the main rivers. If uniform precipitation is considered, the most important zones of high erosion potential of the Venezuelan Andes are located in the central Chama and Santo Domingo valleys, with secondary regions of high erosion potential on both the northern and southern flanks. Consequently, under this assumption the Chama and Santo Domingo rivers, together with the small catchments (Tucaní, San Pedro, Mimbós) on the northwest flank of the orogen, have high relative erosion indexes (whether considering TSP, USP or SSP) with the peripheral Coloncito and Agua Viva-Chejendé River catchments showing lower erosion indexes (Table 2).

When the precipitation data are incorporated in the erosion index predictions, the results differ significantly because of the strong orographic effect (Figure 4B), with maximum erosion potential shifting to the southeastern flank of the mountain belt (Figure 6). In particular, the predicted high relative erosion index in the central Chama River valley disappears when precipitation is taken into account, due to the pronounced aridity of this valley. Consequently, the southeast-draining Santo Domingo catchment is predicted to have the highest relative

erosion index (whether considering TSP, USP or SSP), followed by the Chama River catchment. Incorporating spatially variable precipitation lowers the relative erosion index values for the small northwestern Tucaní, San Pedro and Mimbós catchments, which become indistinguishable from those for the peripheral Agua Viva-Chejendé and Coloncito catchments (Table 2).

5. DISCUSSION: RELATIONS BETWEEN TECTONICS, CLIMATE AND EROSION IN THE VENEZUELAN ANDES

Whether long-term exhumation rates in mountain belts are controlled to first order by tectonic or climatic factors remains a matter of debate. Some authors have argued for strong coupling between long-term exhumation and precipitation, for instance for the Central Andes (Montgomery et al., 2001), Washington Cascades (Reiners et al., 2003), while others argued for decoupling between long-term exhumation and precipitation, such as in the central Himalaya (Burbank et al., 2003) or in the European Alps (Vernon et al., 2009). Recently, Mora et al. (2008) have argued for coupling between precipitation and exhumation rates in the Eastern Cordillera of Colombia, which is contiguous to the Venezuelan Andes. Can long-term exhumation rates in the Venezuelan Andes be correlated to present-day precipitation rates? If they are uncorrelated with precipitation, what could be the controlling factor driving exhumation? The underlying question is, how strongly are tectonic and climatic processes coupled and on which timescales? Table 2 summarizes our observations on long-term exhumation, predicted short-term erosion potential and potential controlling factors for the seven studied catchments in the Venezuelan Andes. The challenge lies in comparing exhumation rates over several millions of years, derived from detrital AFT ages, with present-day precipitation or seismicity data that was collected over the past 100 years or less.

In order to gain insight into the potential controls on erosion and exhumation rates in the Venezuelan Andes, we have calculated Pearsonian correlation coefficients between each of the measures reported in Table 2. Table 3 summarizes the results of this analysis. Given that we compare all variables for seven catchments, correlations are statistically significant (at a 95% confidence level) for a Pearson correlation coefficient $r \geq 0.7$.

Figure 7 shows how long-term exhumation rates in the Venezuelan Andes correlate with different potential control parameters (present-day relief, precipitation, seismic energy release, seismic strain rate and stream power). A first observation is the very strong positive correlation (r = 0.88) between long-term exhumation rates and relief, implying that the present-day relief of the Venezuelan Andes is adapted to the long-term exhumation rates. The correlation we find here is much stronger than that reported, for instance, in the European Alps (Wittmann et al., 2007; Vernon et al., 2009) or in the San Bernardino Mountains of California (Binnie et al., 2007). The reason for this is probably the comparably lower exhumation rates and relief in the Venezuelan Andes, so that bedrock landsliding on threshold slopes, which tends to decouple relief and exhumation rates (Montgomery and Brandon, 2002) is less important with respect to these other mountain belts. In effect, a large proportion of slopes close to the threshold for landsliding is only encountered in the central Sierra Nevada and Sierra la Culata blocks of the Venezuelan Andes (Bermúdez et al., 2010).

In contrast, long-term exhumation rates appear to be decoupled from present-day precipitation rates; they appear even (weakly) negatively correlated with present-day precipitation (i.e. highest exhumation rates occur on the dry northwest flank of the orogen). Also, whereas short-term erosion indexes (*EI*) are not correlated to long-term exhumation rates for any of the

three models (i.e. TSP, SSP or USP), the correlations become even weaker or negative when spatially variable precipitation rates are taken into account in the calculation of these measures (EI_p). The lack of correlations suggests that the present-day precipitation pattern does not strongly control long-term exhumation rates in the Venezuelan Andes, in contrast to what has been inferred for the contiguous Eastern Cordillera of Colombia (Mora et al., 2008). However, two caveats need to be recalled before concluding from this data that climate and exhumation are decoupled in the Venezuelan Andes. First, the relatively limited spatial extent of our sampled catchments, for which the wet southern flank is clearly under-represented, and second the timescale problem mentioned previously. Considering the first, it is clear that our dataset would benefit from inclusion of additional remote south-flank catchments. As for the problem of comparing measurements on strongly varying timescales, whereas we obviously acknowledge that we cannot readily extrapolate the present-day precipitation measurements several million years into the past, we do note that (1) the Neogene sedimentary record of northern South America suggests that the topographic relief of the Venezuelan Andes, and therefore its associated orographic imprint, has been in place since Late Miocene times (Hoorn et al., 1995; Díaz de Gamero, 1996); and (2) Quaternary glaciations, which may strongly modify erosion patterns in some mountain belts (e.g., Burbank et al., 2003; Gabet et al., 2008; Vernon et al., 2009) have been relatively limited in the Venezuelan Andes (Schubert, 1984; Stansell et al., 2006). It has been suggested, both in the Andes and elsewhere (e.g., Bookhagen et al., 2005; Abbühl et al., 2010), that spatial patterns of erosion are strongly by the occurrence of extreme events, leading to decoupling between patterns of erosion and present-day average climate. This could be the case in the Venezuelan Andes, but sufficient resolution in the regional climate record to address this question is currently lacking.

In order to assess potential tectonic controls on long-term exhumation rates, we use cumulative seismic energy release and seismic strain rate as proxies for tectonic forcing (Tables 2 and 3). We estimate the cumulative seismic energy released within the different catchment in two different ways: by averaging the values of Figure 5B within each catchment, or by simply summing the seismic energy released by each earthquake within the catchment boundaries and normalising by catchment area. The difference between the two methods is the extent to which earthquakes occurring outside the catchment boundaries are taken into account.

The inferred seismic energy release correlates weakly to moderately with either catchment-averaged exhumation rate or 10 km-radius relief, with *r*-values varying between 0.40 and 0.64 (Table 3). As noted previously, the pattern of seismic energy release is strongly controlled by large ($M_l > 5$) strike-slip earthquakes located outside the Venezuelan Andes, which contribute significantly to accumulated seismic energy in the low-exhumation Agua Viva-Chejendé catchment for instance. The seismic energy release only integrates a century of data and, similar to the precipitation records, may therefore not be directly comparable to long-term exhumation rates and relief. However, there is very little correlation either between measures of seismic energy release and stream-power based erosion indexes, suggesting that short-term erosion rates (if these are correctly predicted by the stream-power models) are decoupled from seismic energy release.

In contrast to the pattern of released seismic energy, the inferred seismic strain rate correlates very strongly with both catchment-averaged exhumation rates (r = 0.81) and 10 km-radius relief (r = 0.85). Catchments on the northwest flank of the orogen that show the largest seismic strain rates (Mimbós, San Pedro, Coloncito; ~10^{-15} s^{-1}) are also characterized by the

highest relief (> 1650 m) and exhumation rates (> 0.4 km Myr^{-1}). In contrast, the northwestern Agua Viva-Chejendé catchment, which has the lowest relief and exhumation rates, also shows very low seismic strain rates (2.5×10^{-17} s^{-1}).

Our data thus suggest that active tectonic deformation of the Venezuelan Andes provides a much stronger control on long-term exhumation rates throughout the orogen than the pattern of precipitation. It also suggests that the widely used stream-power based erosion potential does not adequately model erosion rates throughout the mountain belt. The reason for this may be that the simple stream-power expression does not take into account the effects of sediment flux, stochasticity of discharge and incision thresholds (e.g., Whipple, 2004; Lague, 2010). We have previously suggested an overall tectonic control on relief and exhumation rates in the Venezuelan Andes as the orogen can be divided in fault-bounded blocks that each have their characteristic relief and exhumation history (Bermúdez et al., 2010), as also observed in other obliquely convergent mountain belts (e.g., Spotila et al., 2007). It would be interesting to map out erosion rates throughout the Venezuelan Andes using cosmogenic nuclides in stream sediments in order to analyse whether the same patterns emerge on shorter time scales.

6. CONCLUSIONS

Detrital AFT analysis of modern river sediment provides an efficient tool for studying long-term exhumation rates in complex areas with difficult access, such as the Venezuelan Andes. We have shown that the technique efficiently records average catchment-wide long-term exhumation rates when compared to *in-situ* samples. The detrital AFT ages of seven major catchments of the Venezuelan Andes reproduce and extrapolate the exhumation patterns

reported by Bermúdez et al. (2010; 2011) and can thus be used to infer exhumation rates in areas where *in-situ* data is absent. Our results suggest that using weighted average exhumation rates, in order to include the effect that rapidly exhuming areas of a catchment have higher sediment yields improves both the fit to observed detrital age distributions and the correlations with potential control parameters.

Catchment-averaged long-term exhumation rates in the Venezuelan Andes are fairly constant at 0.31-0.48 km Myr^{-1}. Rates are higher (>0.4 km Myr^{-1}) on the northwestern flank of the mountain belt (Mimbós, San Pedro, Tucani and Coloncito rivers), whereas they are lowest (0.31 km Myr^{-1}) in the northeastern Agua Viva-Chejendé catchment. The large Chama and Santo Domingo catchments draining the central Venezuelan Andes show intermediate rates of 0.37-0.38 km Myr^{-1}. Average exhumation rates correlate very well with relief of the catchments as well as with seismic strain rates, but correlations with both stream-power based predictions of short-term erosion potential and precipitation are weak or negative.

The lack of correlation between long-term exhumation rates and relief, on the one hand, and precipitation on the other suggests that either precipitation is not the main controlling factor for driving exhumation and relief development in the Venezuelan Andes, or that the short-term record of present-day precipitation is not representative of long-term average values. Alternatively, erosion may be effectively controlled by extreme climate events that are not captured by the record. A moderate correlation with seismic energy release indicates that the 100-year seismic record does not fully capture the current deformation, because of the long recurrence time of large seismic events. However, we show that calculating the seismic strain rate and its extrapolation over geologic time is feasible and allows studying relationships between long-term exhumation rate, relief and tectonics. Our study suggests that the climatic

control on exhumation rates in the active orogens of northern South America may have been overstated. Climatic variations appear to only have a second-order control on relief, erosion, and long-term exhumation rates, as has been suggested elsewhere (e.g. Riebe et al., 2001a,b; Kirchner et al., 2001).

ACKNOWLEDGEMENTS

This study was supported by the CDCH de la Universidad Central de Venezuela (UCV), Project Number PI 08-00-6219-2006 and ECOS-Nord project V08U01. We thank Juan Flores and Antonio León for support during fieldwork. We acknowledge Dr. Gerhard Kopp of the Institute for Meteorology and Climate Research, University of Karlsruhe, Germany, for providing the meteorological data of the Mérida Atmospheric Research Station for Pico Espejo (MARS). María Elena Naranjo of the Universidad de Los Andes (ULA) provided precipitation data of the following stations: Páramo de Mucuchies, Páramo Pico El Aguila, Los Plantíos, Mucubají, Valle Grande and Tabay. FUNVISIS provided access to the seismicity data. Finally, we thank Jean Braun and Christoph Glotzbach for discussion and assistance during the writing of this manuscript, and Bodo Bookhagen and an anonymous reviewer for constructive comments.

REFERENCES CITED

Abbühl, L.M., Norton, K.P., Schlunegger, F., Kracht, O., Aldahan, A., and Possnert, G., 2010, El Niño forcing on ^{10}Be-based surface denudation rates in the northwestern Peruvian Andes?: Geomorphology, v. 123, p. 257-268, doi: 10.1016/j.geomorph.2010.07.017.

Aleman, A., and Ramos, V.A., 2000, Northern Andes, in Cordani, U.G., Milani, E.J., Thomaz Filho, A., and Campos, D.A., eds., Tectonic Evolution of South America: Rio de Janeiro, Companhia de Pesquisa de Recursos Minerais / Serviço Geológico do Brasil, p. 453-480.

Arya, S., Mount, D.M., Netanyahu, N.S., Silverman, R., and Wu, A., 1998, An optimal algorithm for approximate nearest neighbor searching in fixed dimensions: Journal of the Association for Computing Machinery,, v. 45, p. 891–923.

Audemard, F.A., 1997, Holocene and historical earthquakes on the Boconó fault system, southern Venezuelan Andes: Trench confirmation: Journal of Geodynamics, v. 24, p. 155–167.

Audemard, F.A., Machette, M.N., Cox, J.W., Dart, R.L and Haller, K.M., 2000, Map and Database of Quaternary Faults in Venezuela and its Offshore Regions: USGS Open-File Report 00–018 (paper edition).

Backé, G., Dhont, D., and Hervouët, Y., 2006, Spatial and temporal relationships between compression, strike-slip and extension in the Central Venezuelan Andes: Clues for Plio-Quaternary tectonic escape: Tectonophysics, v. 425, p. 25–53.

Bermúdez, M.A., Kohn, B.P., van der Beek, P.A., Bernet, M., O'Sullivan, P.B and Shagam, R., 2010, Spatial and temporal patterns of exhumation across the Venezuelan Andes: Implications for Cenozoic Caribbean geodynamics: Tectonics, v. 29, TC5009, doi:10.1029/2009TC002635.

Bermúdez, M.A., van der Beek, P., and Bernet, M., 2011, Asynchronous Miocene-Pliocene exhumation of the central Venezuelan Andes: Geology, v. 39, p. 139–142.

Bernet, M., Brandon, M.T., Garver, J.I. and Molitor, B., 2004, Fundamentals of detrital zircon fission-track analysis for provenance and exhumation studies with examples from the European Alps: Geological Society of America Special Paper, v. 378, p. 25–36.

Binnie, S.A., Phillips, W.M., Summerfield, M.A. and Fifield, L.K., 2007, Tectonic uplift, threshold hillslopes, and denudation rates in a developing mountain range: Geology v. 35, p. 743–746.

Bookhagen, B., Thiede, R.C., and Strecker, M.R., 2005, Late Quaternary intensified monsoon phases control landscape evolution in the northwest Himalaya: Geology, v. 33, p. 149-152, doi: 10.1130/g20982.1.

Bookhagen, B. and Strecker, M.R., 2008, Orographic barriers, high-resolution TRMM precipitation, and relief variations along the eastern Andes: Geophysical Research Letters, v. 35, L06403, doi: 10.1029/2007GL032011.

Brandon, M.T., 1992, Decomposition of fission-track grain-age distributions: American Journal of Science, v. 292, p. 535–564.

Brandon, M.T., 1996, Probability density plots for fission-track grain age distributions: Radiation Measurements, v. 26, p. 663–676.

Brandon, M.T., and Vance, J.A., 1992, Tectonic evolution of the Cenozoic Olympic subduction complex, Washington State, as deduced from fission track ages for detrital zircons: American Journal of Science, v. 292, p. 565–636.

Brandon, M.T., Roden-Tice, M.K., and Garver, J.I., 1998, Late Cenozoic exhumation of the Cascadia accretionary wedge in the Olympic Mountains, northwest Washington State: Geological Society of America Bulletin, v. 110, p. 985–1009.

Braun, J., Burbidge, D.R., Gesto, F.N., Sandiford, M., Gleadow, A.J.W., Kohn, B.P., and Cummins, P.R., 2009, Constraints on the current rate of deformation and surface uplift of the Australian Continent from a new seismic database and low-T thermochronological data: Australian Journal of Earth Sciences, v. 56, p. 99–110.

Brewer, I.D., Burbank, D.W. and Hodges, K.V., 2006, Downstream development of a detrital cooling-age signal: Geological Society of America Special Paper, v. 398, p. 321–338.

Burbank, D.W., Blythe, A.E., Putkonen, J., Pratt-Sitaula, B., Gabet, E., Oskin, M., Barros, A., and Ojha, T.P., 2003, Decoupling of erosion and precipitation in the Himalayas: Nature, v. 426, p. 652–655.

Carter, A., 2007, Heavy minerals and detrital fission-track thermochronology: Developments in Sedimentology, v. 58, p. 851–868.

Case, J.E., Shagam, R. and Giegengack, R.F., 1990, Geology of the Northern Andes; an overview: The Geology of North America, v. H, p. 177–200.

Cediel, F., Shaw, R.P., and Cáceres, C., 2003, Tectonic assembly of the Northern Andean Block: American Association of Petroleum Geologists Bulletin, v. 79, p. 815–848.

Champagnac, J.-D., Molnar, P., Sue, C. and Herman, F., 2012, Tectonics, climate, and mountain topography: Journal of Geophysical Research, v. 117, B02403, doi: 10.1029/2011jb008348.

Colletta, B., Roure, F., De Toni, B., Loureiro, D., Passalacqua, H., and Gou, Y., 1997, Tectonic inheritance, crustal architecture, and contrasting structural styles in the Venezuela Andes: Tectonics, v. 16, p. 777–794, doi: 10.1029/97TC01659.

Colmenares, L., and Zoback, M.D., 2003, Stress field and seismotectonics of northern South America: Geology, v. 31, p. 721–724.

Conover, W. J., 1980, Practical Nonparametric Statistics: 2nd ed. Wiley, New York, 493 pp.

Corredor, F., 2003, Seismic strain rates and distributed continental deformation in the northern Andes and three-dimensional seismotectonics of northwestern South America: Tectonophysics, v. 372, p. 147–166.

Cortés, M., and Angelier, J., 2005, Current states of stress in the northern Andes as indicated by focal mechanisms of earthquakes: Tectonophysics, v. 403, p. 29–58.

Dadson S.J., Hovius N., Chen H., Dade W.B., Hsieh M.-L., Willett S.D., Hu J.-C., Horng M.-J., Chen M.-C., Stark C.P., Lague D., and Lin J.-C. 2003, Links between erosion, runoff variability and seismicity in the Taiwan orogen: Nature, v. 426, p. 648–651, doi: 10.1038/nature02150.

Dewey, J.W., 1972, Seismicity and tectonics of western Venezuela: Bull. Seism. Soc. America, v. 62, p. 1711–1751.

Díaz de Gamero, M.L., 1996, The changing course of the Orinoco River during the Neogene: a review: Palaeogeography, Palaeoclimatology, Palaeoecology, v. 123, p. 385–402.

Dodson, M.H., 1973, Closure temperature in cooling geochronological and petrological systems: Contributions to Mineral Petrology, v. 40, p. 259–274.

Egbue, O. and Kellogg, J., 2010, Pleistocene to Present North Andean "escape": Tectonophysics, v. 489, p. 248–257, doi: 10.1016/j.tecto.2010.04.021.

Ehlers, T. A., 2005, Crustal thermal processes and the interpretation of thermochronometer data: in T. Ehlers and P. W. Reiners (Eds.), Low Temperature Thermochronometry: Techniques, Interpretations, and Applications: Reviews in Mineralogy and Geochemistry, v. 58, p. 315–350.

Farías, M., Charrier, R., Carretier, S., Martinod, J., Fock, A., Campbell, D., Cáceres, J., and Comte, D., 2008, Late Miocene high and rapid surface uplift and its erosional response in the Andes of central Chile (33°–35°S): Tectonics, v. 27, TC1005, doi: 10.1029/2006TC002046.

Finlayson, D.P., Montgomery, D.R., and Hallet B., 2002, Spatial coincidence of rapid inferred erosion with toung metamorphic massifs in the Himalayas: Geology, v. 30, p. 219–222.

Foster, D., Brocklehurst, S.H. and Gawthorpe, R.L., 2008, Small valley glaciers and the effectiveness of the glacial buzzsaw in the northern Basin and Range, USA: Geomorphology, v. 102, p. 624–639, doi: 10.1016/j.geomorph.2008.06.009.

Gabet, E.J., Burbank, D.W., Pratt-Sitaula, B., Putkonen, J. and Bookhagen, B., 2008, Modern erosion rates in the High Himalayas of Nepal: Earth and Planetary Science Letters, v. 267, 482–494.

Garver, J.I,, Brandon, M.T,, Roden-Tice, M.K,, Kamp, P.J.J., 1999, Exhumation history of orogenic highlands determined by detrital fission track thermochronology: Geological Society of London, Special Publications, v. 154, p. 283–304.

Glotzbach, C., van der Beek, P.A., and Spiegel, C., 2011, Episodic exhumation and relief growth in the Mont Blanc massif, Western Alps from numerical modelling of thermochronology data: Earth and Planetary Science Letters, v. 304, p. 417–430.

Glotzbach, C., van der Beek, P.A., Carcaillet, J., and Delunel, R., in review, Deciphering the driving forces of short-term denudation in glacially impacted landscapes, an example from the Western Alps: Journal of Geophysical Research – Earth Surface.

Gutenberg, B, and Richter, C.F., 1954, Seismicity of the Earth and Associated Phenomena: Princeton University Press, Princeton, New Jersey, 245 pp.

Holt, W.E., Shen-Tu, B., Haines, J. and Jackson, J., 2000, On the determination of self-consistent strain rate fields within zones of distributed continental deformation, In: The History and Dynamics of Global Plate Motions: AGU Geophysical Monograph Series, v. 121, 113–141.

Hoorn, C., Guerrero J., Sarmiento G.A., and Lorente, M.A., 1995, Andean tectonics as a cause for changing drainage patterns in Miocene northern South America: Geology, v. 23, p. 237–240.

Jarvis, A., Reuter, H.I. , Nelson, A., and Guevara, E., 2008, Hole-filled SRTM for the globe Version 4, available from the CGIAR-CSI SRTM 90m Database (http://srtm.csi.cgiar.org).

Kirchner, J. W., Finkel, R. C., Riebe, C. S., Granger, D. E., Clayton, J. L., King, J. G., and Megahan, W.F., 2001, Mountain erosion over 10 yr, 10 k.y., and 10 m.y. time scales: Geology, v. 29, p. 591–594.

Kohn, B.P., Shagam, R., Banks, P.O., and Burkley, L.A., 1984, Mesozoic-Pleistocene fission track ages on rocks of the Venezuelan Andes and their tectonic implications: Geological Society of America Memoir 162, p. 365–384.

Koons, P.O., 2009, On the implications of low spatial correlation of tectonic and climate variables in the western European Alps: Geology, v. 37, p. 863–864.

Lamb, S. and Davis, P., 2003, Cenozoic climate change as a possible cause for the rise of the Andes: Nature, v. 425, p. 792–797.

Lague, D., 2010, Reduction of long-term bedrock incision efficiency by short-term alluvial cover intermittency: Journal of Geophysical Research, v. 115, F02011, doi: 10.1029/2008jf001210.

McPhillips, D. and Brandon, M.T., 2010, Using tracer thermochronology to measure modern relief change in the Sierra Nevada, California. Earth and Planetary Science Letters, v. 296, p. 373–383, doi: 10.1016/j.epsl.2010.05.022.

Mitchell, S.G. and Montgomery, D.R., 2006, Influence of a glacial buzzsaw on the height and morphology of the Cascade Range in central Washington State, USA: Quaternary Research, v. 65, p. 96–107.

Molnar, P. and England, P., 1990, Late Cenozoic uplift of mountain ranges and global climate change: chicken or egg?: Nature, v. 346, p. 29–34.

Montgomery, D.R., Balco, G., and Willett, S.D., 2001, Climate, tectonics, and the morphology of the Andes: Geology, v. 29, p. 579–582.

Montgomery, D.R., Brandon, M.T., 2002, Topographic controls on erosion rates in tectonically active mountain ranges: Earth and Planetary Science Letters, v. 201, p. 481–489.

Mora, A., Parra, M., Strecker, M.R., Sobel, E.R., Hooghiemstra, H., Torres, V., and Jaramillo, J.V., 2008, Climatic forcing of asymmetric orogenic evolution in the Eastern Cordillera of Colombia: Geological Society of America Bulletin, v.120, p. 930–949.

Mora, A., Gaona, T., Kley, J., Montoya, D., Parra, M., Quiroz, L.I., Reyes, G., and Strecker, M.R., 2009, The role of inherited extensional fault segmentation and linkage in contractional orogenesis: a reconstruction of Lower Cretaceous inverted rift basins in the Eastern Cordillera of Colombia: Basin Research, v. 21, p. 111-137.

Naranjo, M.E., and Duque, R., 2004, Estimación de la oferta de agua superficial y conflictos de uso en la cuenca alta del Río Chama, Mérida, Venezuela: INCI, v. 29, p. 130–137.

Niu, F., Bravo, T., Pavlis, G., Vernon, F., Rendon, H., Bezada, M., and Levander, A., 2007, Receiver function study of the crustal structure of the southeastern Caribbean plate boundary and Venezuela: Journal of Geophysical Research, v. 112, B11308, doi: 10.1029/2006JB004802.

Parra, M., Mora, A., Sobel, E.R., Strecker, M.R., and Gonzalez, R., 2009, Episodic orogenic front migration in the northern Andes: Constraints from low-temperature thermochronology in the Eastern Cordillera, Colombia: Tectonics, v. 28, doi: 10.1029/2008TC002423.

Pindell, J.L., and Kennan, L., 2001, Kinematic evolution of the Gulf of Mexico and Caribbean, in Fillon, R.H., Rosen, N.C., and Weimer, P., eds., Petroleum Systems of Deep-Water Basins: Global and Gulf of Mexico Experience: GCSSEPM Foundation, 21st Annual Research Conference, Transactions: Houston, TX, Gulf Coast Section, Society for Sedimentary Geology, p. 193–220.

Rahl, J.M., Ehlers, T.A. and van der Pluijm, B.A., 2007, Quantifying transient erosion of orogens with detrital thermochronology from syntectonic basin deposits: Earth and Planetary Science Letters, v. 256, p. 147–161.

Reiners, P. W., and Brandon, M.T., 2006, Using thermochronology to understand orogenic erosion: Annual Reviews Earth Planetary Sciences, v. 34, p. 419–466.

Reiners, P. W., Ehlers, T. A., Mitchell, S.G., and Montgomery, D.R., 2003, Coupled spatial variations in precipitation and long-term erosion rates across the Washington Cascades: Nature, v. 426, p. 645–647.

Riebe, C. S., Kirchner, J. W., Granger, D. E., and Finkel, R. C., 2001a, Minimal climatic control on erosion rates in the Sierra Nevada, California: Geology, v. 29, p. 447–450.

Riebe, C. S., Kirchner, J. W., Granger, D. E., and Finkel, R. C., 2001b, Strong tectonic and weak climatic control of long-term chemical weathering rates: Geology, v. 29, p. 511–514.

Ruhl, K.W., and Hodges, K.V., 2005, The use of detrital mineral cooling ages to evaluate steady state assumptions in active orogens: An example from the central Nepalese Himalaya: Tectonics, v. 24, TC4015, doi:10.1029/2004TC001712.

Schneider J. F., Pennington W. D., and Meyer R. P., 1987, Microseismicity and focal mechanisms of the intermediate depth Bucaramanga Nest, Colombia: Journal of Geophysical Research, v. 92, p.13913–13926.

Schubert, C., 1984, The Pleistocene and recent extent of the glaciers of the Sierra Nevada de Merida, Venezuela: Erdwissenschaftliche Forschung , v. 18, p. 269–278.

Spotila, J.A., House, M.A., Niemi, N.A., Brady, R.C., Oskin, M. and Buscher, J.T., 2007, Patterns of bedrock uplift along the San Andreas fault and implications for mechanisms of transpresion: In A.B. Till, S.M. Roeske, J.C. Sample and D.A. Foster (Eds.), Exhumation Associated with Continental Strike-Slip Fault Systems: Geological Society of America Special Paper, v. 434, p. 15–33.

Stansell, N.D., Polyssar, P.J., and Abbott, M.B., 2006, Last glacial maximum equilibrium-line altitude and paleo-temperature reconstructions for the Cordillera de Mérida, Venezuelan Andes: Quaternary Research, v. 67, p. 115–127.

Stewart, R.J. and Brandon, M.T., 2004, Detrital-zircon fission-track ages for the "Hoh Formation": Implications for late Cenozoic evolution of the Cascadia subduction wedge: Geological Society of America Bulletin, v.116, p. 60–75.

Stock, G.M., Ehlers, T.A. and Farley, K.A., 2006, Where does sediment come from? Quantifying catchment erosion with detrital apatite (U-Th)/He thermochronometry: Geology, v. 34, p. 725–728.

Strecker, M.R. Alonso, R.N., Bookhagen, B., Carrapa, B., Hilley, G.E., Sobel, E.R., and Trauth, M.H., 2007, Tectonics and climate of the southern central Andes. Annual Review of Earth and Planetary Sciences, v. 35, p. 747–787.

Strecker, M.R., Alonso, R., Bookhagen, B., Carrapa, B., Coutand, I., Hain, M.P., Hilley, G.E., Mortimer, E., Schoenbohm, L., and Sobel, E.R., 2009,. Does the topographic distribution of the central Andean Puna Plateau result from climatic or geodynamic processes?: Geology, v. 37, p. 643–646.

Thomson, S.N., Brandon, M.T., Tomkin, J.H., Reiners, P.W., Vasquez, C. and Wilson, N.J., 2010, Glaciation as a destructive and constructive control on mountain building: Nature, v. 467, p. 313–317, doi: 10.1038/nature09365

Tranel, L.M., Spotila, J.A., Kowalewski, M.J. and Waller, C.M., 2011, Spatial variation of erosion in a small, glaciated basin in the Teton Range, Wyoming, based on detrital apatite (U-Th)/He thermochronology: Basin Research, v. 23, p. 571–590,10.1111/j.1365-2117.2011.00502.x.

Tucker, G.E., and Whipple, K.X., 2002, Topographic outcomes predicted by stream erosion models: Sensitivity analysis and intermodel comparison: Journal of Geophysical Research, v. 107, B9, 2179, doi:10.1029/2001JB000162.

van der Hilst, R., and Mann, P., 1994, Tectonic implications of tomographic images of subducted lithosphere beneath northwestern South America: Geology, v. 22, p. 451-454.

Vermeesch, P., 2007, Quantitative geomorphology of the White Mountains (California) using detrital apatite fission track thermochronology: Journal of Geophysical Research, v. 112, F03004, doi: 10.1029/2006JF000671.

Vernon, A.J., van der Beek, P.A., and Sinclair, H., 2009, Spatial correlation between long-term exhumation rates and present-day forcing parameters in the western European Alps: Geology, v. 37, p. 859–862.

Whipp, D.M. Jr., Ehlers, T.A., Braun, J., and Spath, C.D., 2009, Effect of exhumation kinematics and topographic evolution on detrital thermochronometer data: Journal of Geophysical Research, v. 114, F04014, doi:10.1029/2008JF001195.

Whipple, K.X., 2004, Bedrock rivers and the geomorphology of active orogens: Annual Review of Earth and Planetary Sciences, v.32, p. 151–185.

Whipple, K.X., 2009, The influence of climate on the tectonic evolution of mountain belts: Nature Geoscience, v. 2, p. 97–104.

Williamson, J.H., 1968, Least-squares fitting of a straight line: Canadian Journal of Physics, v. 46, p.1845–1847.

Wilson, J.P., Gallant, J.C., 2000, Terrain Analysis: Principles and Applications: John Wiley & Sons, Inc, 479 p.

Wittmann, H., von Blanckenburg, F., Kruesmann, T., Norton, K.P. and Kubik, P.W., 2007, The relation between rock uplift and denudation from cosmogenic nuclides in river sediment in the Central Alps of Switzerland: Journal of Geophysical Research, v. 112, F04010, doi:10.1029/2006JF000729.

Wobus, C.W., Whipple, K.X., Kirby, E., Snyder, N.P., Johnson, J., Spyropolou, K., Crosby, B. and Sheehan, D., 2006, Tectonics from topography: procedures, promise and pitfalls: In S. Willett, N. Hovius, M. Brandon and D. Fisher (Editors), Tectonics, Climate and Landscape Evolution: Geological Society of America Special Paper, v. 398, p. 55–74.

Figure captions

Fig. 1. A) Shaded digital elevation model (1-km resolution; Jarvis et al., 2008) showing tectonic framework of northwestern South America. Col = Colombia; Ec = Ecuador; NAB = Northern Andean Block; VA = Venezuelan Andes; BFS = Boconó fault; MB = Maracaibo Block (Modified from Cediel et al., 2003). B) Geologic, structural and drainage map of the Venezuelan Andes, modified from Case et al. (1990), Audemard et al. (2000) and Bermúdez et al. (2010). Major fault systems are indicated (IFS: Icotea; BFS: Boconó; CSAFS: Central-Sur Andino; CFS: Caparo; VFS: Valera and BurF: Burbusay). Inset shows major tectonic blocks of the Venezuelan Andes (CATB: Cerro Azul Thrust; CB: Caparo; EB: Escalante; ECB: El Carmen; SLCB: Sierra La Culata; SNB: Sierra Nevada, and TB: Trujillo). C) Simplified structural cross section of central Venezuelan Andes. SLC: Sierra La Culata, SN: Sierra Nevada de Mérida (Modified from Colletta et al., 1997).

Fig. 2. Shaded 90-m resolution digital elevation model of the Venezuelan Andes (Jarvis et al., 2008) with location of bedrock apatite fission-track ages (white circles) and detrital samples (star symbols). Thick dark gray polygons indicate catchment boundaries. Histograms show distribution of detrital AFT ages for the different samples (note logarithmic age scale); the grain-age distributions were decomposed into peak age components using binomial peak fitting (Stewart and Brandon, 2004). Peak ages (P1, P2, P3) are indicated, with the number of grains (percentage in parentheses) that composes each population.

Fig. 3. Comparison of measured (continuous black line; dashed lines indicate 95% confidence limits) and predicted bedrock (grey lines indicate 1000 random samples) cumulative density age functions (CDF) for the Chama catchment; inset shows probability-density functions (PDF) for comparison. (A) shows a comparison for random (un-weighted) sampling of bedrock age distribution; (B) shows results for a weighted age distribution where the probability of sampling a particular bedrock age is a function of the associated long-term exhumation rate relative to the average exhumation rate (see text for discussion). Numbers show average Kolmogorov Smirnov (KS) and Kuiper (KT) statistics, with associated p-values, which test the null hypothesis (H_0: the distributions are indistinguishable). The number of simulations that fail the KS and KT test at a significance level $p = 0.05$ is also indicated.

Fig. 4. (A) 5-km radius relief across the Venezuelan Andes, draped over a shaded relief image. Peaks over 4300 m elevation in the central part of the range are indicated by triangles. Mean relief for each analyzed catchment is summarized in Table 2. (B) Average precipitation pattern (m yr^{-1}) across the Venezuelan Andes, compiled from various databases (see text for details), overlain on shaded relief image of topography

Fig. 5. (A) Major active faults systems (modified from Audemard et al., 2000) and seismicity database compiled for the period 1911-2011 from digital libraries at Universidad de Los Andes (http://lgula.ciens.ula.ve/) and FUNVISIS (http://www.funvisis.org.ve). (B) Cumulated seismic energy released, calculated from the earthquake database. Individual earthquakes with $M > 5$ occurring outside the Venezuelan Andes are indicated (1: 1993/12/31, 70.70 W / 9.65 N, $M_w = 5.4$; 2: 2001/12/21, 70.96 W / 8.17 N, $M_w = 5.6$; 3: 2006/01/03, 71.92 W /9.89 N, $M_w = 5.0$; 4: 2006/08/04, 70.65 W / 9.97 N, $M_w = 5.2$; 5: 1995/12/29, 70.26 W / 9.75 N, $M_w = 5.3$; 6: 1998/02/12, -70.23 W / 9.14 N, $M_w = 5.6$). (C) Seismic strain rate as predicted from the distribution and magnitude of earthquakes and the maximum earthquake magnitude M_{max}, of each catchment using a 0.5° × 0.5° binning of the data (see text for explanation).

Fig. 6. Average logarithmic stream power index maps across the Venezuelan Andes. Left columns (A, C and E) take spatially variable precipitation into account (stream power calculated following equation 7); right columns (B, D, F) assume spatially constant precipitation (stream power calculated following equation 6): A, B) Total Stream Power (TSP; $m = n = 1$ in equations 6, 7); C, D) Unit Stream Power (USP; $m = 0.5$; $n = 1$); E, F) Shear Stress (SSP; $m = 0.33$; $n = 0.67$).

Fig. 7. Correlation plots for: A) 5-km relief, B) present-day precipitation, C) seismic energy release, D) seismic strain rate, E) Total stream power (uniform precipitation) and F) Total stream power (spatially variable precipitation), all versus exhumation rate. Released seismic energy was calculated from the map of cumulated seismic energy release within 25-km radius windows around each earthquake (Figure 3B). Seismic strain rate was calculated only for catchments with more than 10 earthquakes following equation (4) in the text. For all correlations, r is the correlation coefficient calculated for a least-square regression line

without considering errors bars, and r_w is the correlation coefficient calculated for the Williamson (1968) regression line.

Supplementary Material

Figure S1. Cumulative density plots of single-grain ages for the seven catchments analyzed in this study.

Table S1. Results of Kolmogorov-Smirnov equality test for the cumulative density distributions of single-grain ages of different catchments shown in Figure S1. For each couple of catchments, the KS-statistic and the corresponding *p*-value testing the null-hypothesis that the sample distributions are different are given. In blue, comparisons that pass the KS-test (i.e. have similar age distributions), in bold red font, comparisons that fail the KS-test.

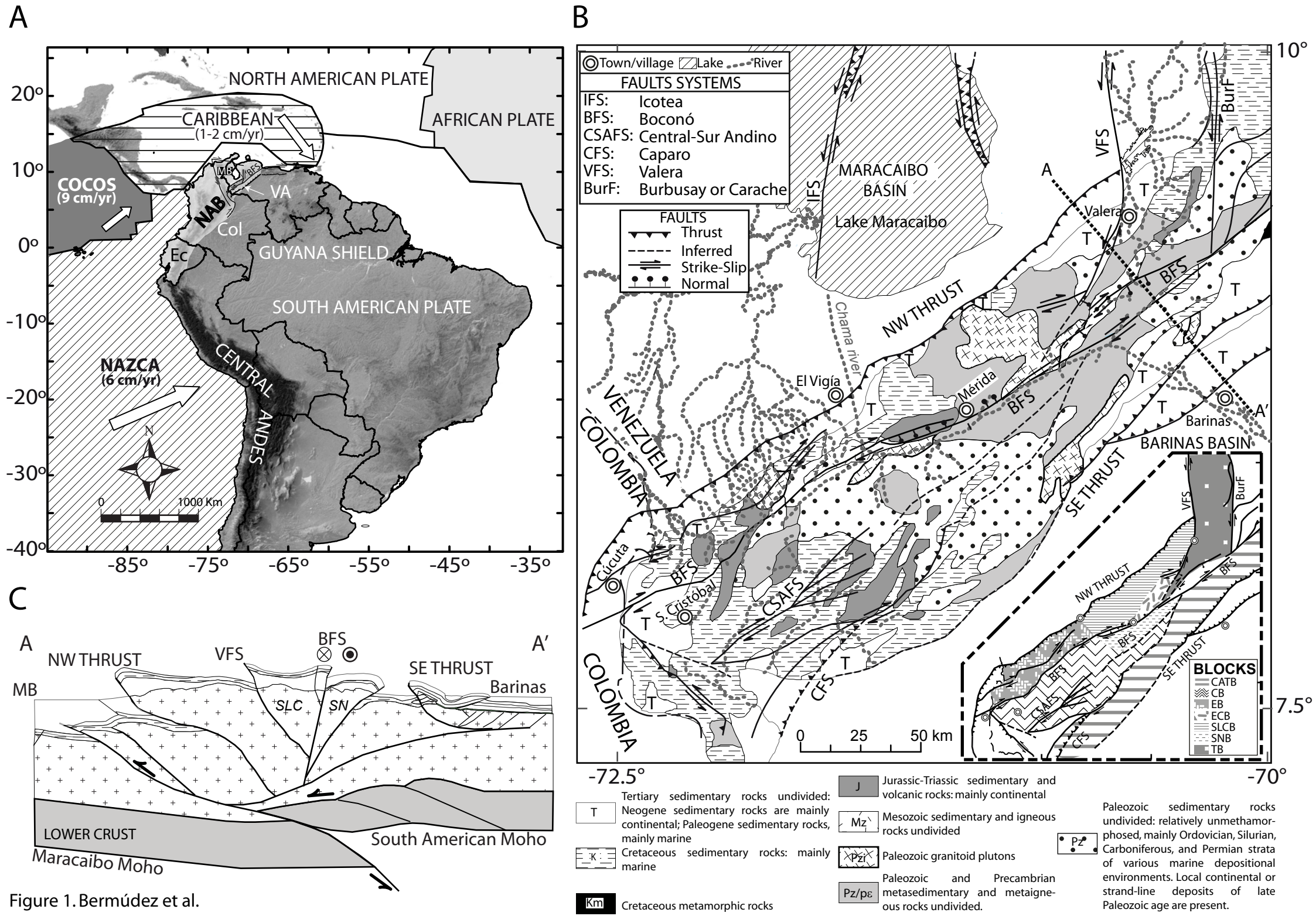

Figure 1. Bermúdez et al.

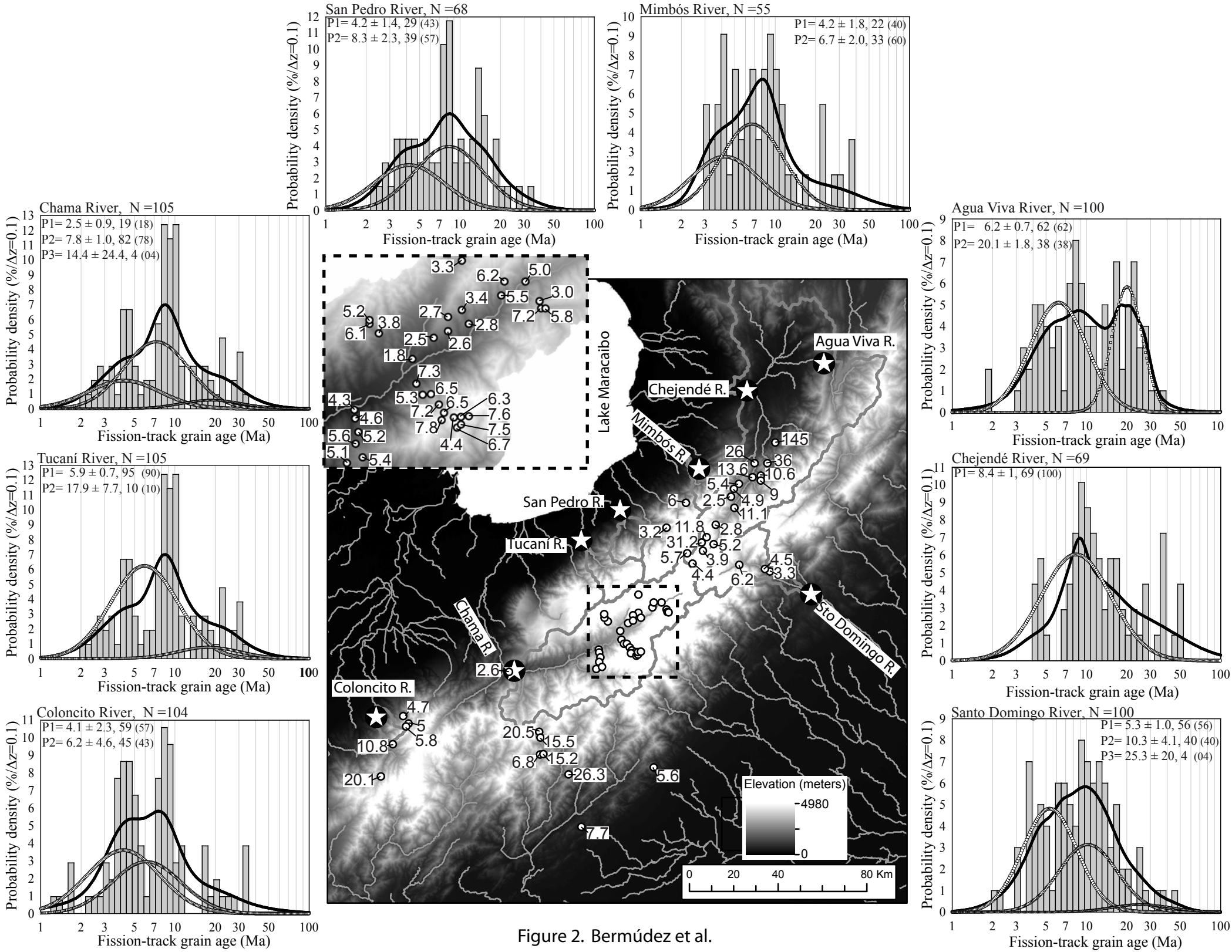

Figure 2. Bermúdez et al.

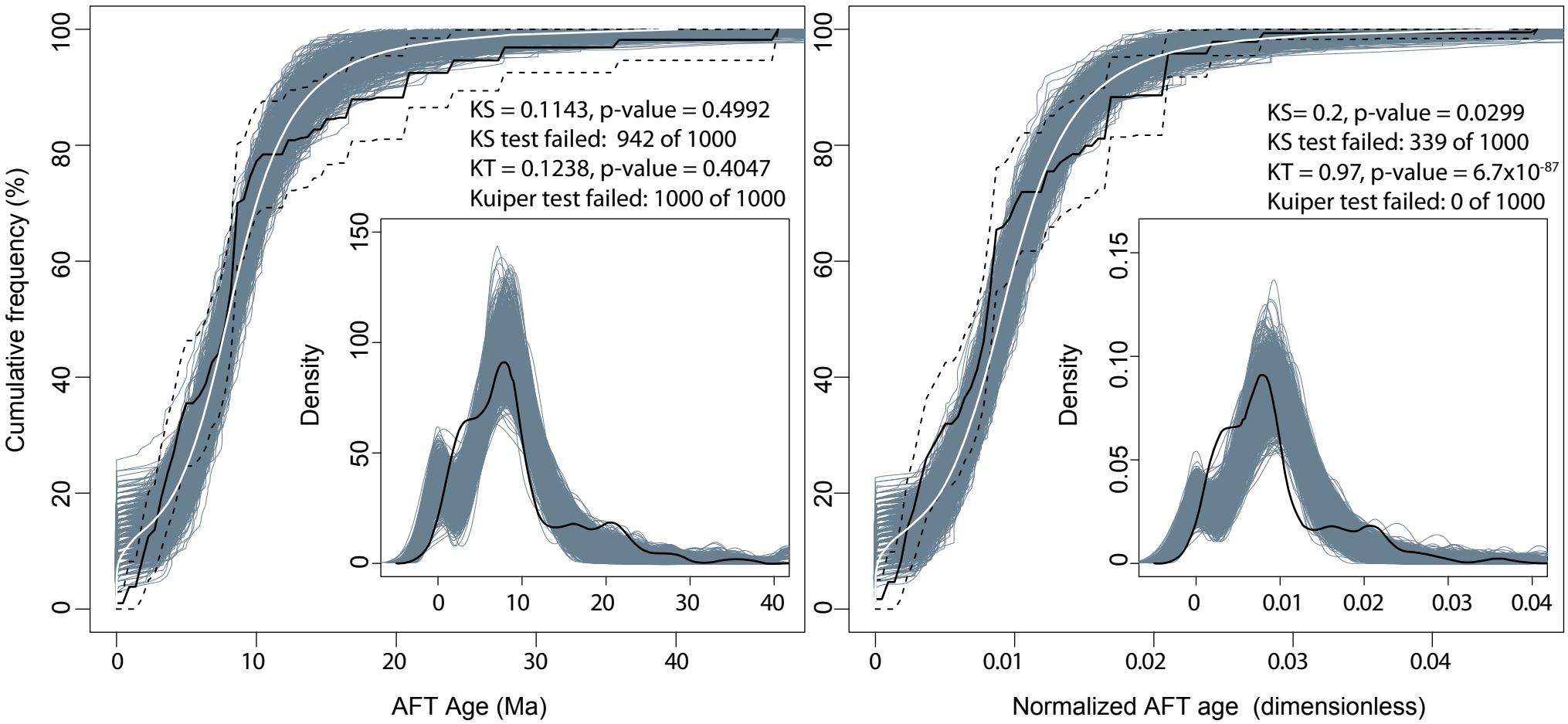

Figure 3. Bermúdez et al.

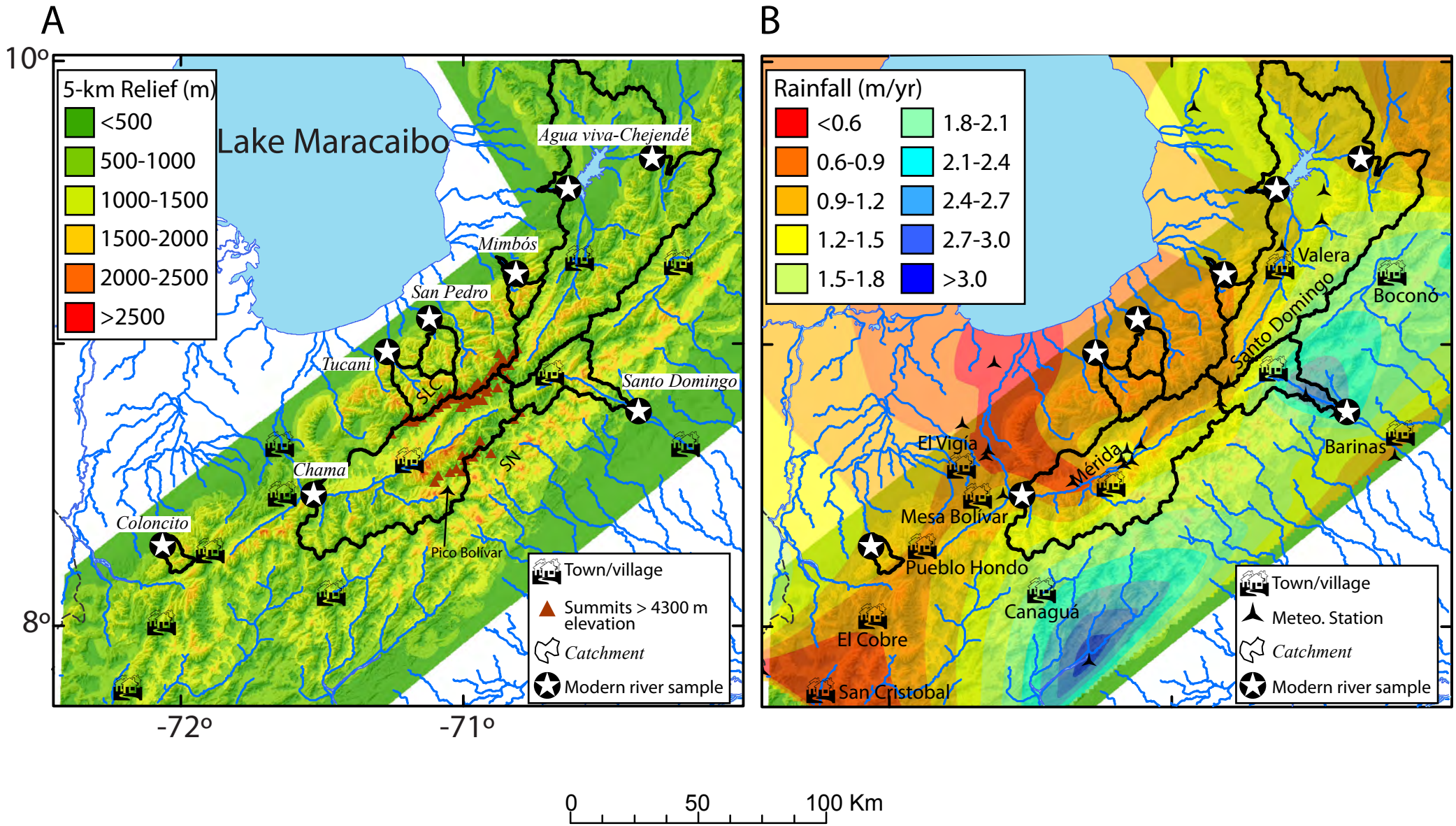

Figure 4. Bermúdez et al.

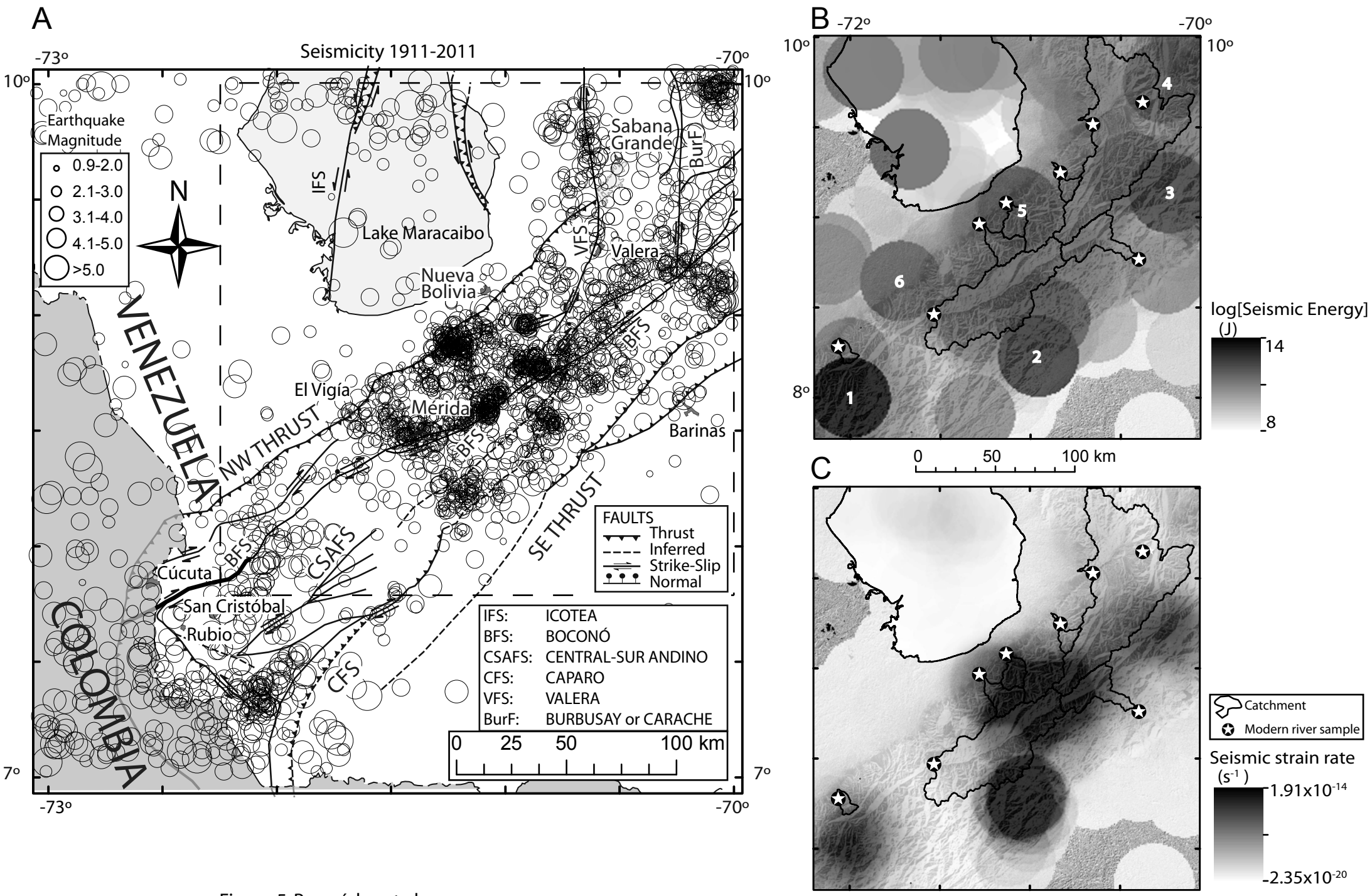

Figure 5. Bermúdez et al.

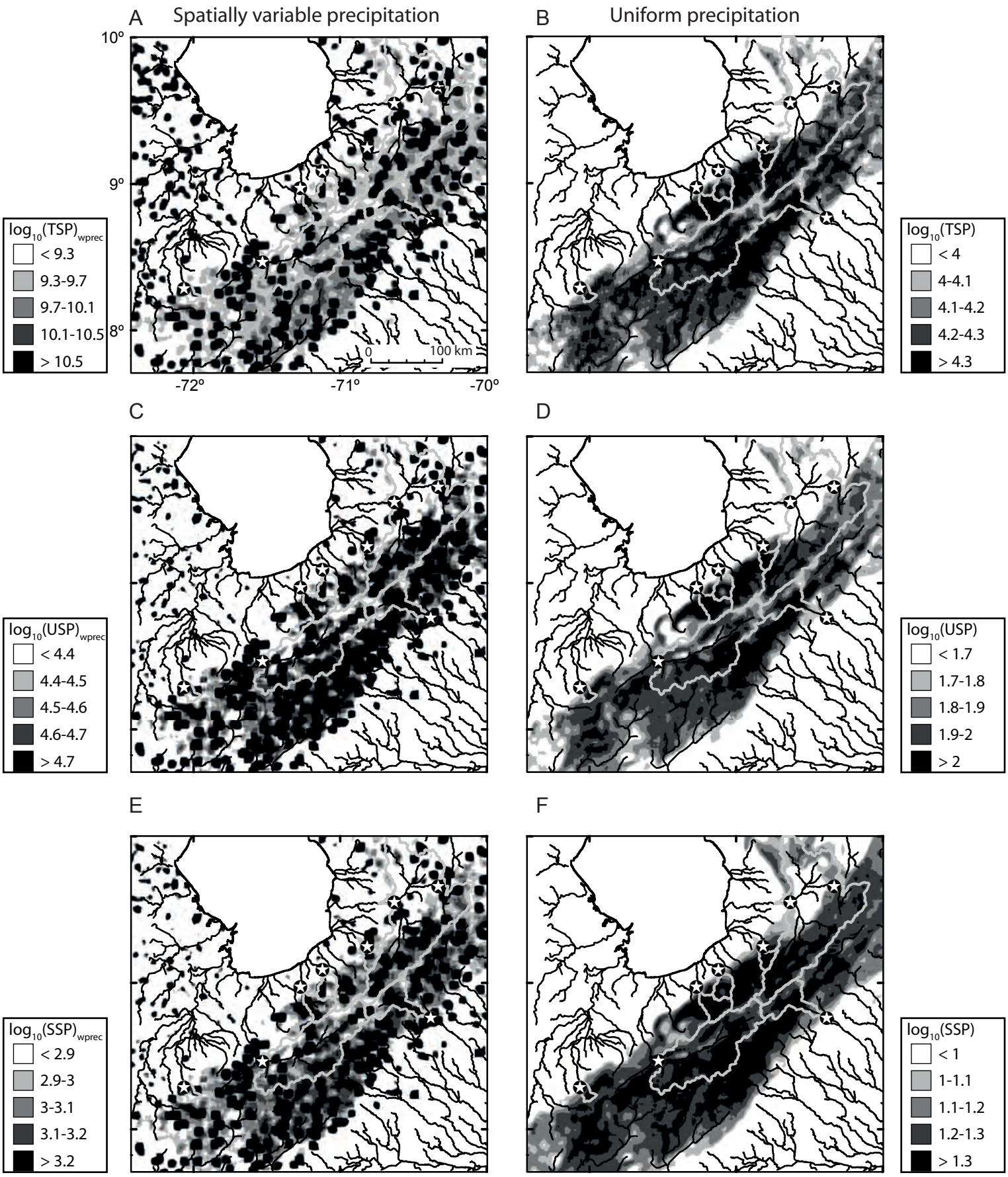

Figure 6. Bermúdez et al.

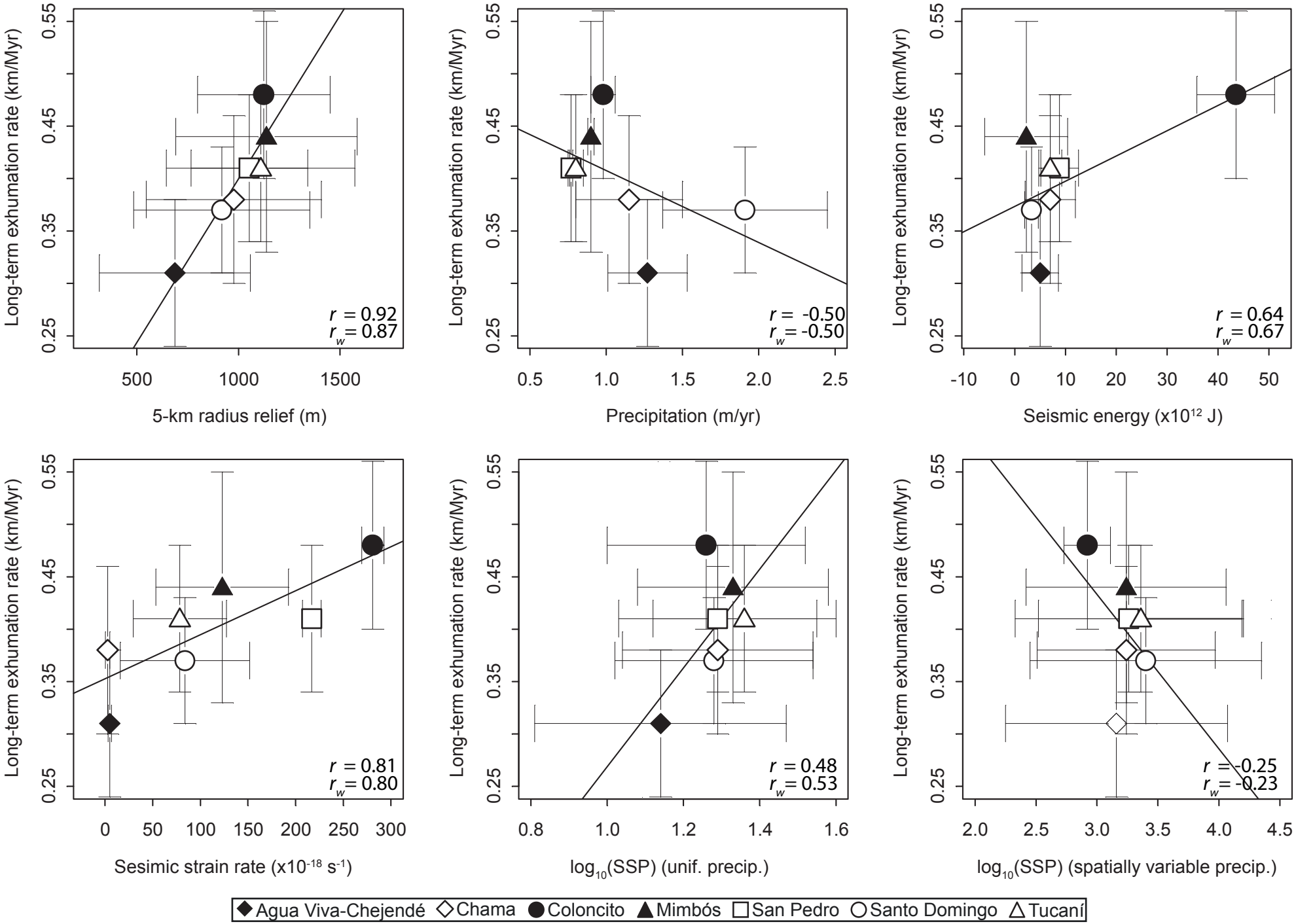

Fig. 7. Bermúdez et al.

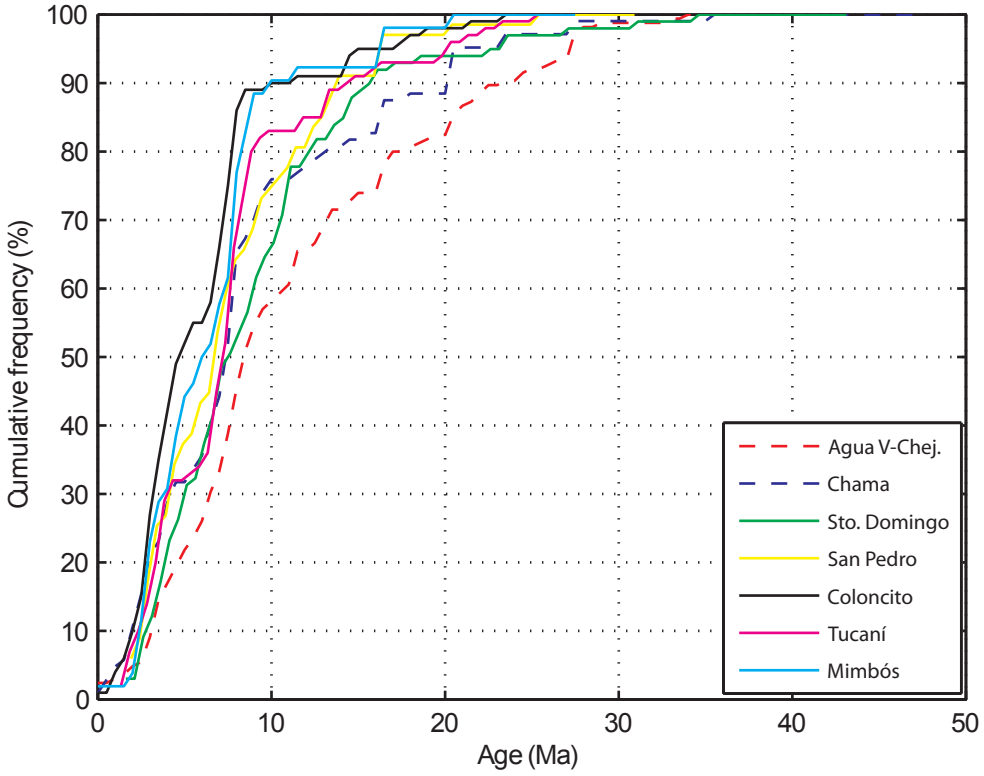
Cumulative frequency (%)
Age (Ma)
0
10
20
30
40
50
60
70
80
90
100
Agua V-Chej.
Chama
Sto. Domingo
San Pedro
Coloncito
Tucaní
Mimbós